

Soft, elastic, water-repellent materials

Martin Coux, Christophe Clanet, and David Quéré

Citation: *Appl. Phys. Lett.* **110**, 251605 (2017); doi: 10.1063/1.4985011

View online: <http://dx.doi.org/10.1063/1.4985011>

View Table of Contents: <http://aip.scitation.org/toc/apl/110/25>

Published by the [American Institute of Physics](#)



**THE WORLD'S RESOURCE FOR
VARIABLE TEMPERATURE
SOLID STATE CHARACTERIZATION**



OPTICAL STUDIES SYSTEMS



SEEBECK STUDIES SYSTEMS



MICROPROBE STATIONS



HALL EFFECT STUDY SYSTEMS AND MAGNETS



WWW.MMR-TECH.COM

Soft, elastic, water-repellent materials

Martin Coux, Christophe Clanet, and David Quéré

Physique & Mécanique des Milieux Hétérogènes, UMR 7636 du CNRS, ESPCI, 75005 Paris, France and LadHyX, UMR 7646 du CNRS, École Polytechnique, 91128 Palaiseau, France

(Received 26 April 2017; accepted 24 May 2017; published online 23 June 2017)

Small hydrophobic textures at solid surfaces provide water repellency, a situation whose detailed properties critically depend on the geometry of textures. Depending on their size, density, and shape, water slip, rain repellency, or antifogging can be achieved. Here, we discuss how the use of soft, elastic materials allows us to tune reversibly the texture density by stretching or relaxing the materials, which is found to impact water adhesion and rebounds. In addition, solid deformations can also be exploited to largely vary the shape of Wenzel drops, a consequence of the strong pinning of water in this state. *Published by AIP Publishing.* [<http://dx.doi.org/10.1063/1.4985011>]

Wetting of soft materials recently drew much attention, owing to the new situations generated by the interplay between capillarity and elasticity, such as encapsulation,¹ special dissipation,² or self-propulsion.^{3,4} Softness can also be used to stretch or contract solids, for instance, to bend them. These operations hardly affect wettability, since surface chemistry is generally not modified under stresses. The picture should be different in the presence of textures. Textures control wettability, and they are sensitive to the action of stresses. This might affect both the fakir Cassie state⁵ and the impaled Wenzel state,⁶ and possibly induce transitions between them. Up until now, only a few studies have discussed the interactions between the softness of a textured material and its wetting properties. *Zhu et al.* exploited softness for efficiently actuating magnetic pillars⁷ and tilting them in a magnetic field, which generates anisotropic wetting—drops flow more easily along the direction of tilt. *Yao et al.* utilized solid softness with liquid-impregnated textures.⁸ Stretching these materials increases the mutual distance between textures and decreases the height of infused liquid, which modifies the adhesion of drops by a factor up to 5. Closer to what we discuss in this paper, *Lee et al.* considered hydrophobic multi-scale textures on cured polydimethylsiloxane (PDMS).⁹ They show that water repellency is maintained as the material is elongated, yet do not describe how mechanical stresses impact wettability. Our aim here is to show how deformations influence the wetting and conformation of drops placed on soft substrates with pillars.

Soft textured samples are obtained by replicating a hard substrate made of silicon. The matrix is fabricated by classical techniques of lithography and etching.¹⁰ It consists in a square array of cylindrical micropillars, with height $h = 18 \pm 1 \mu\text{m}$, diameter $d = 17.0 \pm 0.5 \mu\text{m}$, and mutual spacing $p = 23 \pm 1 \mu\text{m}$ —all dimensions that compare to that of bumps on lotus leaves.¹¹ The pillar density ϕ_0 is 14%, much smaller than unity as necessary for superhydrophobicity. This surface is molded by PDMS (RTV 615, Momentive Performance Materials), and the mold is silanized with trichloroperfluorooctylsilane (Sigma). We pour vinylpolysiloxane (VPS, Double 8, Zhermack) until forming a layer two millimeters thick and cure it by 20 min of exposure to air. After gently peeling it off, we obtain a soft, elastic, textured surface with

the same geometrical characteristics as its matrix. This material can be stretched and bent, owing to its thinness and to the low elastic modulus of VPS, $E = 250 \pm 15 \text{ kPa}$ (estimated with a standard tensile test). In the range of extension used in this paper, the polymer remains elastic and does not break. Furthermore, VPS is hydrophobic without additional treatment, as shown by water advancing and receding contact angles $\theta_a = 104 \pm 4^\circ$ and $\theta_r = 76 \pm 3^\circ$. On textured VPS, angles jump to typical values in a Cassie state, $\theta_a = 162 \pm 1^\circ$ and $\theta_r = 144 \pm 1^\circ$.

Our experiment consists in stretching the soft, textured material and investigating how this action impacts wettability. The first type of stress is the uniaxial extension sketched in Fig. 1(a). A stripe of textured VPS (dimensions: $5 \text{ cm} \times 2 \text{ cm}$) clamped at both ends is quasi-statically elongated using micrometric screws. The extension ratio $\varepsilon = \ell'/\ell - 1$ is deduced from the dilation of a square drawn on the sample, whose length increases from ℓ to ℓ' as stretching the elastomer. The polymer breaks at $\varepsilon \approx 160\%–180\%$ so that ε was varied between 0 and 153%. We obtain the change of pillar density by measuring the contraction $\varepsilon_\perp = \ell''/\ell - 1$ in the direction perpendicular to extension, where the square contracts by Poisson effect from ℓ to ℓ'' . Typical values of ε and ε_\perp are reported in Table I, together with the relative increase in surface area $\Sigma = (1 + \varepsilon)(1 + \varepsilon_\perp) - 1$ and pillar density $\phi = \phi_0/(1 + \Sigma)$. This density decreases here from $\phi_0 = 14.0\%$ to $\phi = 8.2\%$.

To establish the correspondence between stretching and texture density, we assumed that pillar tops keep a constant diameter as increasing ε . We checked this hypothesis by observing extended samples with a scanning electron microscope (SEM). Figure 1(b) shows both top and side views of pillars, whose mutual distance naturally increases along elongation. However, individual pillars are not strongly affected by tension: even if their base is slightly widened, both the height and top surface area are unchanged. This behavior was found to remain valid up to $\varepsilon = 102\%$, as can be seen in the [supplementary material](#); above this value, direct measurements were impossible to achieve because of the limited size of the cell of visualisation.

We also performed biaxial deformations on square samples with dimensions $5 \text{ cm} \times 5 \text{ cm}$ [Fig. 1(c)]. The four edges

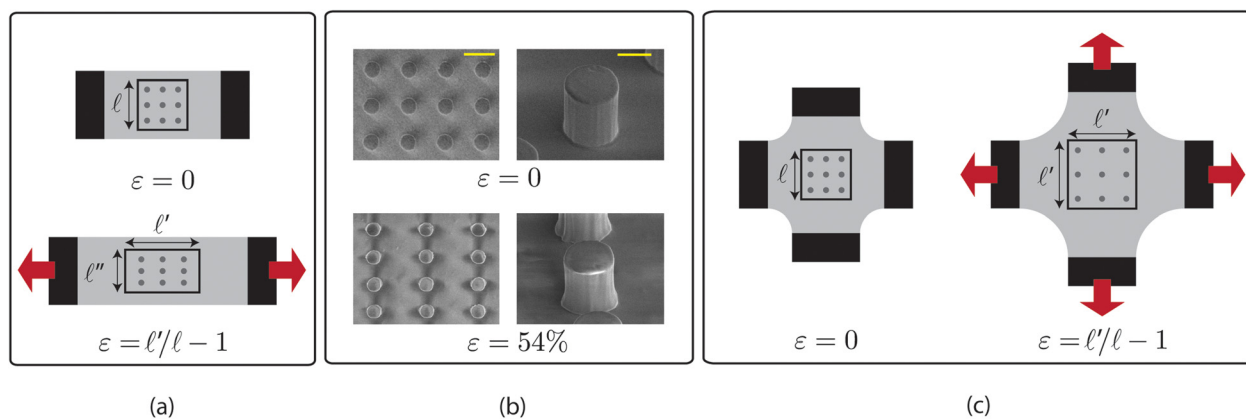


FIG. 1. (a) Uniaxial extension. A stripe of superhydrophobic soft material (light grey) with a square of side ℓ drawn at its center is clamped at its ends (black). The sample is stretched by a quantity $\varepsilon = \ell'/\ell - 1$ and consequently contracts in the perpendicular direction by $\varepsilon_{\perp} = \ell''/\ell - 1$. Surface dilation $\Sigma = \ell'\ell''/\ell^2 - 1$ and pillar density ϕ are calculated assuming a constant surface area of pillars tops (drawn in dark grey). (b) SEM observations of soft superhydrophobic surfaces without ($\varepsilon = 0$) and with uniaxial tension ($\varepsilon = 0.54$). We show both top views and close-ups on single pillars. The scale bars are 25 and 10 μm , respectively. (c) Biaxial extension. A square of superhydrophobic soft material is attached at its four ends and subjected to the same tension on both axes. Extension is $\varepsilon = \ell'/\ell - 1$, and surface dilation is $\Sigma = \ell'^2/\ell^2 - 1$.

TABLE I. Examples of geometrical variations obtained by uniaxial tractions performed on soft VPS.

Extension	0 (%)	1 (%)	2 (%)	3 (%)
ε	0	67	96	153
ε_{\perp}	0	-16	-23	-33
$\Sigma = (1+\varepsilon)(1+\varepsilon_{\perp}) - 1$	0	40	50	70
$\phi = \phi_0/(1+\Sigma)$	14.0	10.0	9.3	8.2

are clamped and deformation is imposed by four sets of micrometric screws. Consequently, the square array of pillars homothetically grows, and it is characterized by a unique extension parameter $\varepsilon = \ell'/\ell - 1$, denoting ℓ and ℓ' as the initial and final size of the square drawn on the sample. As reported in Table II, ε varies between 0 and 57% in this second series of experiments, which makes $\Sigma = (1 + \varepsilon)^2 - 1$ increase from 0 to 146%. This allows us to significantly decrease the density of pillars, from $\phi_0 = 14\%$ without stretch to $\phi = 5.7\%$ at maximum extension. We first privilege this configuration because of its isotropic character, compared to the more anisotropic situation described in Fig. 1(a).

We first wonder how extending the textured material modifies water adhesion and repellency in the Cassie state. We use the classical tilting plate method to quantify the adhesive properties.¹² We gently deposit a controlled volume of water $\Omega = 40 \mu\text{l}$ on the sample and gradually tilt it until the drop departs, at a critical angle α^* . The weight $\rho\Omega g \sin\alpha^*$ is then balanced by the adhesive force $\gamma\pi r \Delta\cos\theta$, denoting γ as the surface tension of water, r as the radius of the circular drop print, and $\Delta\cos\theta$ as the contact angle hysteresis (CAH). By measuring the critical angle α^* ($\approx 10^\circ$ on the sample) and

TABLE II. Examples of geometrical variations obtained after biaxial tractions performed on soft VPS.

Extension	0	1 (%)	2 (%)	3 (%)
ε	0	24	41	57
$\Sigma = (1+\varepsilon)^2 - 1$	0	55	99	146
$\phi = \phi_0/(1+\Sigma)$	14	9	7	5.7

the radius r from side views, we can deduce $\Delta\cos\theta$. Similar measurements are performed after placing the substrate in a given state of extension ε . We observe that water remains in the Cassie state whatever ε , and that the critical angle α^* decreases as the sample is stretched. We display in Fig. 2(a) the variation of CAH as a function of surface dilation Σ . Each data point is obtained after four similar measurements, which yields both an average value and the amplitude of fluctuations.

Hysteresis on the unstretched sample is modest, yet can be significantly lowered (by a factor 2) when dilating the surface (by a factor 2.4). The variation of $\Delta\cos\theta$ with Σ is continuous and slightly non-linear. This behavior can be explained more quantitatively by plotting $\Delta\cos\theta$ as a function of the pillar density ϕ [Fig. 2(b)]. Data are nicely fitted by the function $\phi \ln(\pi/\phi)$ deduced from the Joanny-de Gennes theory of hysteresis on dilute defects.^{13,14} The numerical coefficient used for the fit is 0.3, smaller than found on hard solids where it is close to 1. A smaller coefficient might arise from the use of a soft elastomer, which both softens the pillar edges on which pinning takes place and favors the release of free oligomers likely to lubricate the solid/water contact.¹⁵

Hence, the softness of a textured material allows us to control its adhesion properties: the material is more slippery stretched than relaxed, which we understand from the dilution of textures under extension. We checked that the effect is reversible under cycles of extension ($\Sigma = 33\%$) and relaxation ($\Sigma = 0$). As shown in Fig. 2(c), contact angle hysteresis remains remarkably stable and reproducible along this experiment, where it switches between its values in the relaxed and stretched states. This full reversibility can be maintained as long as the material neither breaks nor undergoes plastic deformations, as it does in our experiments.

In addition to non-adhesiveness, superhydrophobicity in the Cassie state also induces water repellency: impacting drops are reflected by the material, provided their velocity is smaller than some critical value U^* , above which they get partially or even completely stuck. The threshold U^* was shown to be sensitive to the design of the textures,^{16,17} which

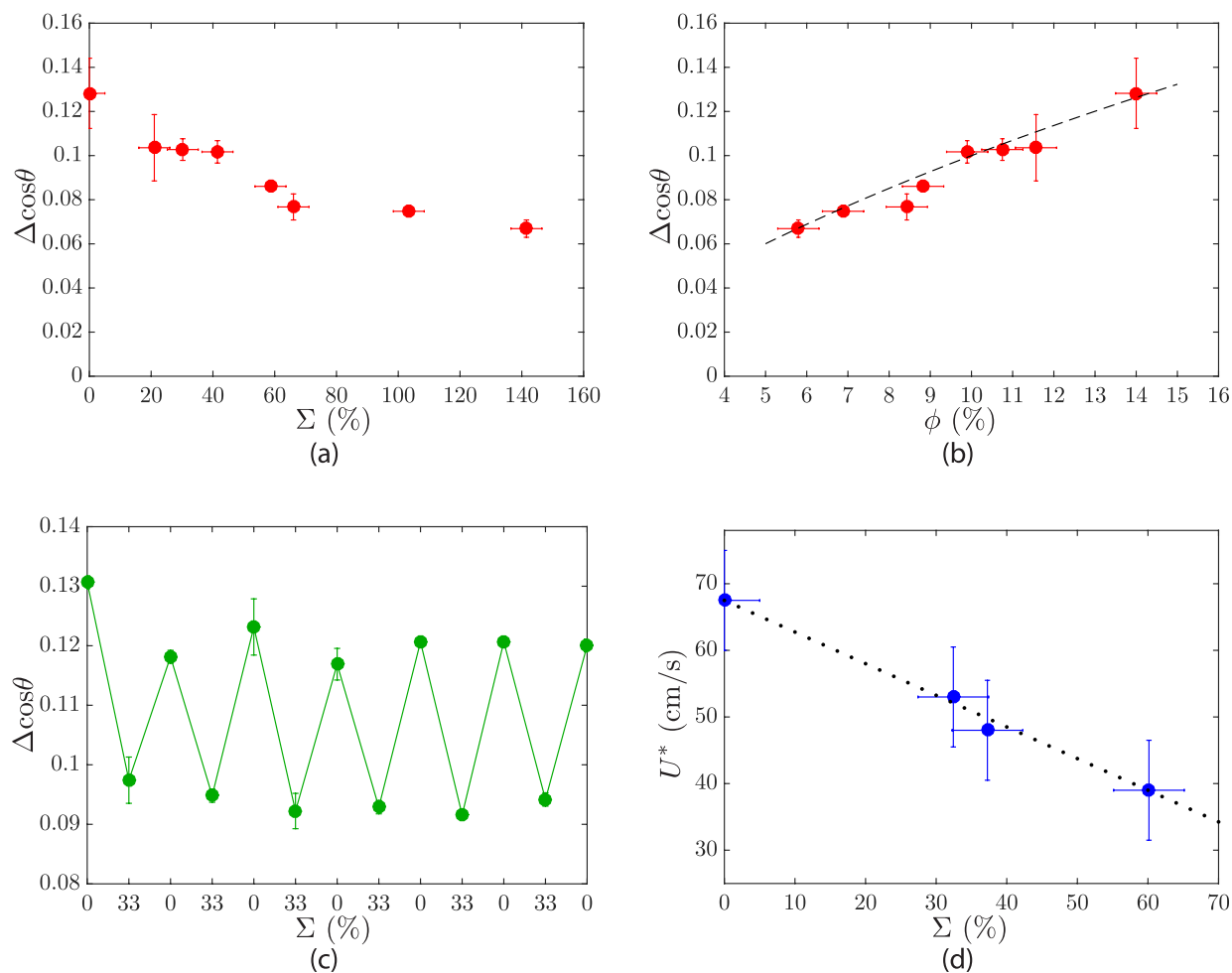


FIG. 2. (a) Contact angle hysteresis in the Cassie state, $\Delta \cos \theta$, on the soft, textured repellent material shown in fig. 1b, as a function of the surface dilation Σ varied by an isotropic extension. (b) Same data presented as a function of the pillar density ϕ . The dashed line shows the function $\Delta \cos \theta = 0.3\phi \ln(\pi/\phi)$ introduced in the text. (c) Variations of $\Delta \cos \theta$ during extension/relaxation cycles, where Σ is alternatively switched between 0% and 33%. (d) Velocity U^* above which impacting drops impale in the texture, and observed here to decrease as the sample is stretched. The dotted line is a guide for the eye.

can be easily understood: on high and dense structures, impacting drops do not contact the solid base where trapping occurs (impalement transition). Our system allows us to vary the texture design through the pillar mutual distance, without affecting other geometrical parameters. As shown in Fig. 2(d), the impalement velocity U^* decreases significantly as the sample is stretched. The spacing between pillars being augmented, impacting drops find more easily the base of the sample where they get trapped. Hence, we can tune the non-adhesive character and the water-repellency of the superhydrophobic surfaces. Interestingly, extending the material improves the first property, whereas it degrades the second one. This suggests that soft textured materials might be used extended for making them slippery, and relaxed under a rain for avoiding water penetration. Therefore, softness can be exploited for implementing contradictory properties on superhydrophobic materials.

We discussed up to now the Cassie state, but soft, textured materials also have advantages in the Wenzel state. Wenzel drops are obtained after an impact at 1 m/s ($> U^*$) on the unstretched material [Fig. 3(a)]. Water meets the solid with an angle $\theta_0 \approx 140^\circ$, corresponding to a radius of contact $r_0 = 1.25$ mm. In order to maximize the deformation, we apply a uniaxial tension, which elongates the drop in the

direction of stretching [Figs. 3(b) and 3(c), showing respectively side and top views].

We observe that the drop never depins, which makes its radius r increase by a factor larger than 2, as reported in Fig. 3(d) with blue data. Consequently, the contact angle θ decreases markedly, from 140° to 60° [Fig. 3(e)]. The latter value remains larger than the receding angle in the Wenzel state ($\sim 40^\circ$), which explains how water can remain pinned all along the experiment. The absence of depinning makes predictable the variations $r(\varepsilon)$ and $\theta(\varepsilon)$. Then, we expect and observe in Fig. 3(d) the reversibility (red data) and a linear variation with slope 1 for $r(\varepsilon)/r_0$ (dashed line). In Fig. 3(e), data nicely compare with the angle calculated for a spherical cap of fixed volume with radius $r = (1 + \varepsilon)r_0$ (dashed line). As shown in the [supplementary material](#), these observations remain valid for biaxial deformations. Hence, the Wenzel state can be exploited to modify mechanically the shape of drops, which can be of interest for generating liquid lenses with a variable focal distance such as discussed in the context of electrowetting.^{18,19}

This situation is specific to highly hysteretic Wenzel states. We show in Figs. 3(f) and 3(g) similar results obtained for flat VPS (green symbols) and textured VPS in the Cassie state (black symbols). Variations are much more

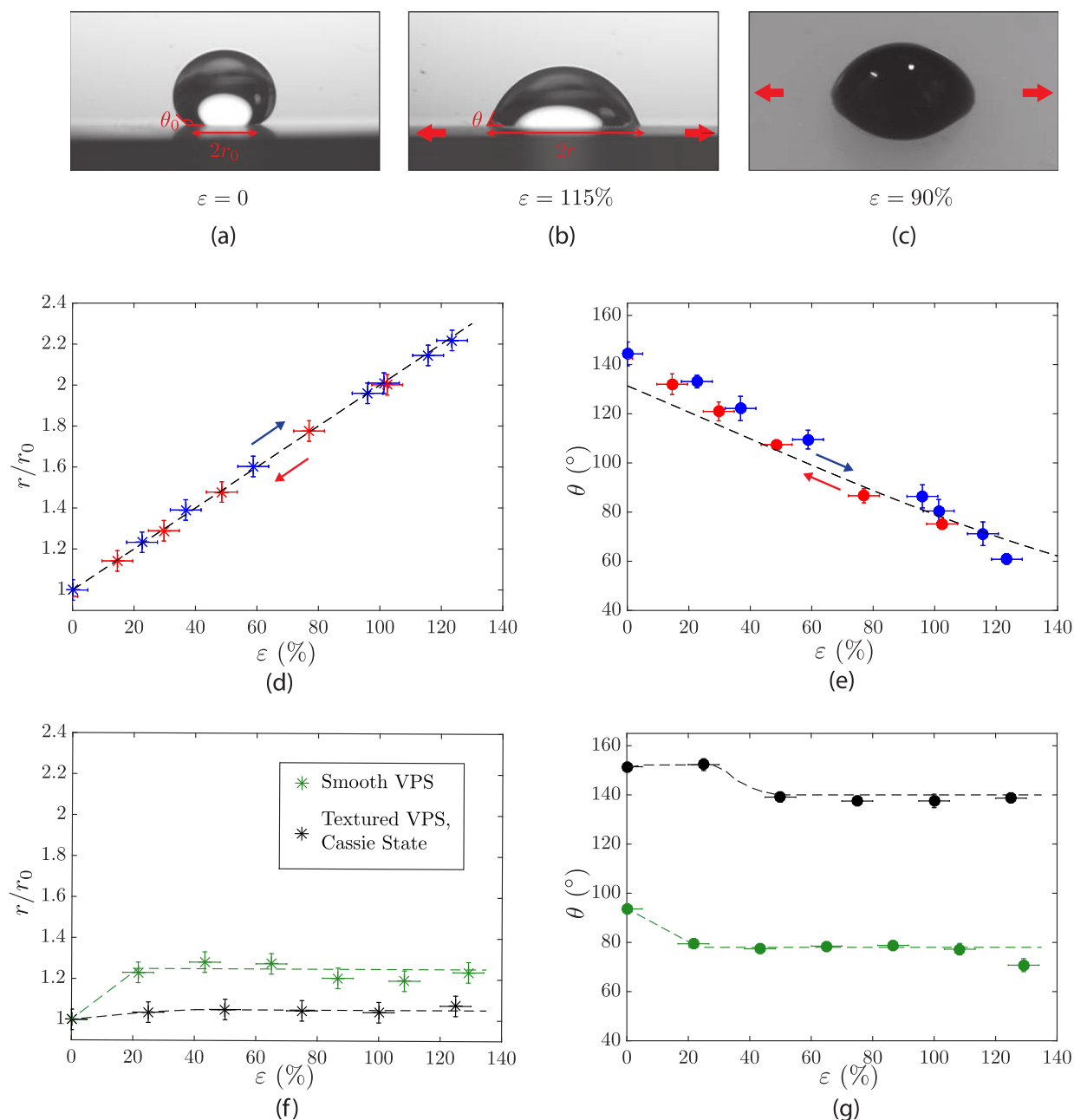


FIG. 3. (a) Water droplet ($\Omega = 20 \mu\text{l}$) in the Wenzel state on an unstretched, soft, elastic, textured surface. We denote its angle and radius of contact as θ_0 and r_0 . (b) and (c) Side and top views of the drop after stretching the substrate by $\varepsilon = 115\%$ (b) and $\varepsilon = 90\%$ (c). (d) and (e) Evolution of the normalized contact radius r/r_0 and contact angle θ as applying a uniaxial cycle of traction (blue data) and retraction (red data), as a function of ε . In (d), the dotted line is a linear fit with slope 1, $r/r_0 = (1 + \varepsilon)$; in (e), the dotted line shows the angle calculated for a spherical cap with radius $r(\varepsilon) = (1 + \varepsilon)r_0$. (f) and (g) Contact size and angle for a uniaxial traction performed on smooth VPS (green data) and on textured VPS in the Cassie state (black data). Dashed lines highlight the “saturation” of the drop shape as $\theta(\varepsilon)$ reaches the receding value θ_r . Water drop still has a volume of $20 \mu\text{l}$.

modest than in Figs. 3(d) and 3(e), because the drop shape now gets “frozen” at small extension, as soon as reaching the receding angle $\theta_r \approx 80^\circ$ (or 140°) on flat (or textured) VPS. Drops depin at further extension, which renders r and θ constant.

In summary, we showed that water on repellent materials can be controlled by playing on the material softness. In the Cassie state, the extension of the substrate dilutes the textures, which yields smaller liquid adhesion and less resistance to impalement. In the Wenzel state, the strong pinning of the contact line makes it possible to change the shape of the impaled liquid, which can be of interest to tune the drop mobility or evaporation. It should be worth studying softer materials, for which we expect both an amplification of our

results, and more complex situations arising from the possibility for drops to modify the textures geometry and arrangement, which can happen if water itself induces significant local deformations. The scale of elasto-capillary deformation is γ/E ($\sim 0.1 \mu\text{m}$ in this study), which becomes on the order of the texture size ($\sim 10 \mu\text{m}$) for solids about 100 times softer—a limit where the physics described here would be deeply modified.

See [supplementary material](#) for a few additional experiments performed either with a harder material or with another type of extension. These experiments complement Figs. 1(b), 2(a), 3(d), and 3(e).

We thank Armel Descamps-Mandine for his help with the SEM observations, and José Bico and Hadrien Bense for useful suggestions.

- ¹C. Py, P. Reverdy, L. Doppler, J. Bico, B. Roman, and C. N. Baroud, *Phys. Rev. Lett.* **98**, 156103 (2007).
- ²S. Karpitschka, S. Das, M. van Gorcum, H. Perrin, B. Andreotti, and J. H. Snoeijer, *Nat. Commun.* **6**, 7891 (2015).
- ³R. W. Style, Y. Che, S. J. Park, B. M. Weon, J. H. Je, C. Hyland, G. K. German, M. P. Power, L. A. Wilen, J. S. Wettlaufer, *et al.*, *Proc. Natl. Acad. Sci.* **110**, 12541 (2013).
- ⁴S. Karpitschka, A. Pandey, L. A. Lubbers, J. H. Weijs, L. Botto, S. Das, B. Andreotti, and J. H. Snoeijer, *Proc. Natl. Acad. Sci.* **113**, 7403 (2016).
- ⁵A. B. D. Cassie and S. Baxter, *Trans. Faraday Soc.* **40**, 546 (1944).
- ⁶R. N. Wenzel, *Ind. Eng. Chem.* **28**, 988 (1936).
- ⁷Y. Zhu, D. S. Antao, R. Xiao, and E. N. Wang, *Adv. Mater.* **26**, 6442 (2014).
- ⁸X. Yao, Y. Hu, A. Grinthal, T. S. Wong, L. Mahadevan, and J. Aizenberg, *Nat. Mater.* **12**, 529 (2013).
- ⁹W. K. Lee, W. B. Jung, S. R. Nagel, and T. W. Odom, *Nano Lett.* **16**, 3774 (2016).
- ¹⁰D. Öner and T. J. McCarthy, *Langmuir* **16**, 7777 (2000).
- ¹¹W. Barthlott and C. Neinhuis, *Planta* **202**, 1 (1997).
- ¹²C. G. L. Fumidge, *J. Colloid Sci.* **17**, 309 (1962).
- ¹³M. Reyssat and D. Quéré, *J. Phys. Chem. B* **113**, 3906 (2009).
- ¹⁴J. F. Joanny and P. G. de Gennes, *J. Chem. Phys.* **81**, 552 (1984).
- ¹⁵A. Hourlier-Fargette, A. Antkowiak, A. Chateauminis, and S. Neukirch, *Soft Matter* **13**, 3484 (2017).
- ¹⁶D. Bartolo, F. Bouamrine, E. Verneuil, A. Buguin, P. Silberzan, and S. Moulinet, *Europhys. Lett.* **74**, 299 (2006).
- ¹⁷M. Reyssat, A. Pépin, F. Marty, Y. Chen, and D. Quéré, *Europhys. Lett.* **74**, 306 (2006).
- ¹⁸B. Berge and J. Peseux, *Eur. Phys. J. E* **3**, 159 (2000).
- ¹⁹C. U. Murade, J. M. Oh, D. van den Ende, and F. Mugele, *Opt. Express* **19**, 15525 (2011).